INTERNATIONAL ATOMIC ENERGY AGENCY
UNITED NATIONS EDUCATIONAL, SCIENTIFIC AND CULTURAL ORGANIZATION
INTERNATIONAL CENTRE FOR THEORETICAL PHYSICS
I.C.T.P., P.O. BOX 586, 34100 TRIESTE, ITALY, CABLE: CENTRATOM TRIESTE

H4.SMR/480-2

**WORKSHOP ON EARTHQUAKE SOURCES & REGIONAL LITHOSPHERIC STRUCTURES FROM SEISMIC WAVE DATA**

**19 - 30 November 1990**

# *SURFACE WAVE HOLOGRAPHY*

**R. SNEIDER**

**Dept. of Theoretical Geophysics**
**University of Utrecht**
**Utrecht, The Netherlands**

*Chapter 14*

# Surface wave holography

*R. Snieder*

## 1. Introduction

Surface waves have proven to be very useful in determining the properties of the Earth's crust and mantle. The traditional surface wave analysis consists of two steps. First, from surface wave recordings, dispersion data (phase velocities or group velocities) are retrieved for each source receiver pair (Dziewonski and Hales, 1972; Nolet, 1977). Next, the information for different frequencies and many source receiver pairs is combined to yield an image of the Earth's interior (e.g. Woodhouse and Dziewonski, 1984; Montagner, 1986; Nataf et al., 1986). These methods implicitly use ray theory by resorting to the "great circle theorem" (Backus, 1964; Jordan, 1978; Dahlen, 1979). This theorem states that for a sufficiently smooth medium the surface wave data are only influenced by the structure under the great circle joining the source and the receiver. The great circle theorem is acceptable provided the inhomogeneity varies little on the scale of the wavelength of the surface waves.

It turns out, however, that this condition is often violated in realistic situations. A Rayleigh wave with a period of 20 seconds has a horizontal wavelength of about 70 kilometers. It is well known that, especially in continents, the lateral heterogeneity on this scale can be considerable. In fact, the models constructed from surface wave data using the great circle theorem sometimes vary strongly on a distance of one wavelength (Panza et al., 1980). In that case the constructed model is inconsistent with the ray theory used for producing the model. It is clear that in these situations one has to resort to a more complete wave theory which takes surface wave scattering and reflection into account. Since these effects are most sensitive to the horizontal *gradient* in the Earth's structure, scattered



*G. Nolet (ed.), Seismic Tomography, 323–337.*




surface waves could provide valuable independent information on the structure of the Earth.

Surface wave scattering and reflection can be treated analytically in two dimensions (Kennett, 1984), but for three dimensional surface wave scattering no analytical solutions are available. In that case one either has to use numerical methods, or make some simplifying assumptions. The Born approximation has been used successfully for describing surface wave scattering in three dimensions (Snieder, 1986ab). A brief outline of this theory is presented in section 2. The Born approximation gives a linear relation between the scattered waves and the heterogeneity. This situation is closely analogous to the wave theories forming the basis of modern migration schemes in exploration geophysics (Clayton and Stolt, 1981; Tarantola, 1984ab; Bleistein et al., 1985; Bleistein and Gray, 1985; Ikelle et al., 1986).

It is therefore not surprising that an inversion scheme using scattered surface waves can be formulated along similar lines. In section 3 it is shown that this scheme can be derived using a least squares criterion, as in Tarantola (1984ab). Without making additional simplifying assumptions the resulting inversion scheme isn't very manageable. It is shown in section 4 how some simplifications result in a workable scheme for reconstructing an inhomogeneity using scattered surface waves. The resulting reconstruction method is similar to holographic techniques used in optics.

In order to check if the method works with real data, a field experiment was conducted on a tidal flat, where surface waves were reflected by a dam. The results for this inversion are presented in section 5. A field experiment, as presented here, is an ideal tool for testing the feasibility of abstract mathematical inversion schemes.

In this chapter the summation convention is used throughout for vector and tensor indices. The dot product which is used is defined by

$$[\mathbf{p}.\mathbf{q}] \equiv p_i^* q_i. \tag{1.1}$$

## 2. Linearized theory for surface wave scattering

The equation of motion combined with the equations for linear elasticity lead to the following expression for the displacement field in the frequency domain

$$L_{ij} u_j = F_i \tag{2.1}$$

where the differential operator L is defined by

$$L_{ij} = -\rho\omega^2 \delta_{ij} - \partial_n c_{inmj} \partial_m \tag{2.2}$$

and F is the point force which excites the wavefield.

Now suppose that the elastic medium (i.e., the density and the elasticity tensor) can be decomposed as follows:

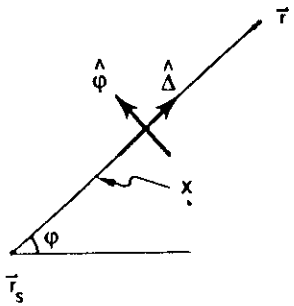


*Figure 1* Definition of the geometric variables for the direct wave.

$$\rho(x,y,z) = \rho^0(z) + \rho^1(x,y,z) \tag{2.3.a}$$

$$\underline{c}(x,y,z) = \underline{c}^0(z) + \underline{c}^1(x,y,z). \tag{2.3.b}$$

This means that the medium is viewed here as a laterally homogeneous reference medium, with heterogeneities superposed on it. This decomposition suggests the following decomposition of the displacement

$$\mathbf{u} = \mathbf{u}^0 + \mathbf{u}^1. \tag{2.4}$$

$\mathbf{u}^0$ is the displacement in the laterally homogeneous reference medium, this term is usually called the direct wave. $\mathbf{u}^1$ describes the effect of inhomogeneities, this term is usually labelled the scattered wave.

In order to derive expressions for $\mathbf{u}^0$ and $\mathbf{u}^1$ it is convenient to introduce the surface wave polarization vectors. For Love waves the polarization vector is

$$\mathbf{p}^\nu(z,\phi) = l_1^\nu(z)\,\hat{\phi} \tag{2.5.a}$$

and for Rayleigh waves

$$\mathbf{p}^\nu(z,\phi) = r_1^\nu(z)\,\hat{\Delta} + i r_2^\nu(z)\,\hat{z}. \tag{2.5.b}$$

In this chapter Greek indices are used to label the surface wave modes. A summation over these indices indicates a summation over both Love waves and Rayleigh waves, thus treating both kinds of waves in an unified way. The unit vectors $\hat{\Delta}$, $\hat{\phi}$ and $\hat{z}$ point respectively in the radial, transverse and down direction, see figure 1. The functions $l_1^\nu(z)$, $r_1^\nu(z)$ and $r_2^\nu(z)$ are the surface wave eigenfunctions as defined in Aki and Richards (1980). These eigenfunctions are assumed to be normalized according to:

$$8 c_\nu U_\nu I_1^\nu = 1 \tag{2.6}$$

$U_\nu$ and $c_\nu$ are the group and phase velocity of the mode under consideration, and $I_1^\nu$ is the kinetic energy integral (Aki and Richards, 1980).

The far field surface wave Green's function of the laterally homogeneous reference medium can conveniently be expressed as a dyad of the polarization vectors. As shown in



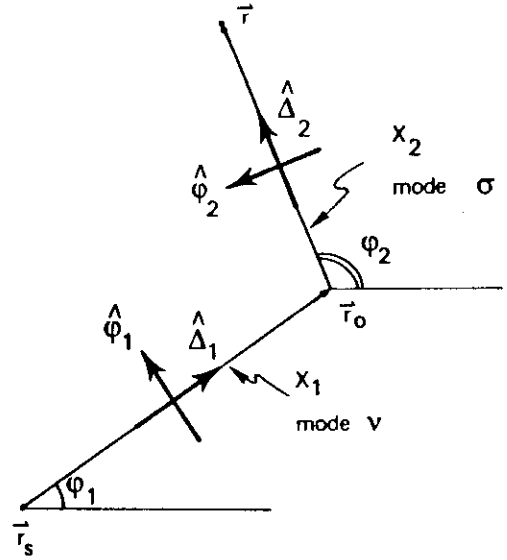


*Figure 2*. Definition of the geometric variables for the scattered wave.

Snieder (1986a), this leads to the following far field expression for the direct wave in the frequency domain

$$\mathbf{u}^0(\mathbf{r}) = \sum_\nu \mathbf{p}^\nu(z,\phi)\,\frac{\exp i(k_\nu X + \frac{\pi}{4})}{(\frac{\pi}{2} k_\nu X)^{1/2}}\,[\mathbf{p}^\nu(z_s,\phi).\mathbf{F}] \tag{2.7}$$

see figure 1 for the definition of the geometric variables. It is assumed here that the wavefield is excited by a point force $\mathbf{F}$ at location $\mathbf{r}_s$. Note that the direct wave is written as a superposition of modes (Love waves and Rayleigh waves), and that the modes don't interact with each other. Using the Born approximation, one can show that for sufficiently weak scatterers the scattered wave in the frequency domain is given by

$$\mathbf{u}^1(\mathbf{r}) = \sum_{\sigma,\nu} \iint \mathbf{p}^\sigma(z,\phi_2)\,\frac{\exp i(k_\sigma X_2 + \frac{\pi}{4})}{(\frac{\pi}{2} k_\sigma X_2)^{1/2}}\,V^{\sigma\nu}(x_0,y_0)\,\frac{\exp i(k_\nu X_1 + \frac{\pi}{4})}{(\frac{\pi}{2} k_\nu X_1)^{1/2}}\,[\mathbf{p}^\nu(z_s,\phi_1).\mathbf{F}]\,dx_0 dy_0 \tag{2.8}$$

see figure 2 for the definition of geometric variables. This expression is derived in Snieder (1986a) for buried scatterers in an isotropic medium. It is shown in Snieder (1986b) that scattering due to surface topography can also be described by (2.8). Reading (2.8) from right to left, one follows the "life history" of the scattered wave. At the source (in $\mathbf{r}_s$), mode

$\nu$ is excited by the projection of the point force $\mathbf{F}$ on the polarization vector $\mathbf{p}^{\nu}$. Then, a propagation to the scatterer occurs. This gives a phase shift and amplitude decay due to geometrical spreading, described by the term $\exp i(k_{\nu}X_1+\frac{\pi}{4})/(\frac{\pi}{2}k_{\nu}X_1)^{\frac{1}{2}}$. At the scatterer (in $\mathbf{r}_0$), scattering and mode conversion occurs. This is described by the interaction terms $V^{\sigma\nu}$. This term gives the coupling between the incoming mode $\nu$, and the outgoing mode $\sigma$. After this, the mode $\sigma$ propagates to the receiver, which is shown by another propagator term. Finally, the oscillation at the receiver (in $\mathbf{r}$) is described by the polarization vector $\mathbf{p}^{\sigma}$. An integration over the scatterer, and a summation over all outgoing and incoming modes $(\sigma,\nu)$ superposes the different parts of the scattered waves $\mathbf{u}^1$.

The interaction terms $V^{\sigma\nu}$ are a linear function of the perturbations in the density ($\rho^1$), the Lame parameters ($\lambda^1$ and $\mu^1$), and the surface topography $h$. It can explicitly be seen that in (2.8) a single scattering approximation is used, since the interaction terms appear only once. For buried inhomogeneities the interaction terms are given in Snieder (1986a), while the interaction terms due to surface topography are derived in Snieder (1986b). For example, the Love wave-Love wave interaction for buried heterogeneities is given by

$$V_{LL}^{\sigma\nu}=\int\left[\left(l_1^{\sigma}l_1^{\nu}\rho^1\omega^2-(\partial_z l_1^{\sigma})(\partial_z l_1^{\nu})\mu^1\right)\cos\phi-k_{\sigma}k_{\nu}l_1^{\sigma}l_1^{\nu}\mu^1\cos 2\phi\right]dz. \qquad (2.9)$$

In this expression $\phi=\phi_2-\phi_1$ is the scattering angle, and $k_{\nu}$ is the wavenumber of mode $\nu$. The interaction terms are a very simple function of the scattering angle $\phi$.

At this point we can already conclude that in inversions using scattered surface waves, we can only obtain information of the scatterers through the interaction terms $V^{\sigma\nu}$. Information at different frequencies (and possibly different modes) is needed to obtain the depth dependence of the inhomogeneities. The dependence of $V^{\sigma\nu}$ on the scattering angle can in principle be used to unravel the contributions from the density and the Lame parameters.

The theory is presented here for a point force excitation in a plane geometry. The excitation by a moment tensor is discussed in Snieder (1986a), and the formulation of this theory in a spherical geometry is shown in Snieder and Nolet (1987). In both cases only minor changes in the theory have to be made.

## 3. A formalism for surface wave holography

Scattered surface waves can be used to map the inhomogeneities in the Earth. The theory in the previous section is linear(ized), therefore least squares inversion techniques can conveniently be used for this. Least squares inversion for variables depending continuously on one or more space variables has been discussed in detail by Tarantola and Valette (1982). Suppose we want to find the following model vector

$$\mathbf{m}(\mathbf{r})=\begin{bmatrix}\rho^1(\mathbf{r})\\ \lambda^1(\mathbf{r})\\ \mu^1(\mathbf{r})\end{bmatrix} \qquad (3.1)$$

and suppose we describe the a-priori knowledge of the heterogeneity with the vector $\mathbf{m}_0(\mathbf{r})$.



Let the vector $\mathbf{u}$ denote all available data in the time domain. With "data" we mean here the difference between the recorded signals, and the synthetics produced by the a-priori model $\mathbf{m}_0(\mathbf{r})$. We shall assume here that the a-priori model is zero ($\mathbf{m}_0(\mathbf{r})=0$). This means that the data ($\mathbf{u}$) consist of the difference between the recorded signals, and the synthetic seismograms of the laterally homogeneous reference medium.

The inversion scheme of Tarantola and Valette (1982) requires the a-priori covariances of the model ($C_m(\mathbf{r},\mathbf{r}')$), and of the data ($C_u$). If the a-priori cross covariances between the model and the data ($C_{um}$) are assumed to vanish, the least squares solution of the model is given by (Tarantola, 1984a):

$$\mathbf{m}=\mathbf{M}^{-1}\,\mathbf{C}_m\,\mathbf{G}^T\,\mathbf{C}_u^{-1}\,\mathbf{u} \qquad (3.2)$$

with

$$\mathbf{M}=\mathbf{C}_m\,\mathbf{G}^T\,\mathbf{C}_u^{-1}\,\mathbf{G}+\mathbf{I} \qquad (3.3)$$

and $G$ is the gradient of the data with respect to the model parameters.

In principle, (3.2) can be used to compute the model $\mathbf{m}(\mathbf{r})$ at every point in three dimensional space. In practice one shouldn't be too optimistic about a straightforward use of (3.2), since three different kinds of inversion are implied in (3.2):

[1] The surface wave energy should be focussed in the horizontal directions on the scatterers.

[2] The contribution of the three parameters $\rho^1$, $\mu^1$ and $\lambda^1$ should be unraveled.

[3] The depth dependence of these parameters should be reconstructed.

It shall be clear that with band limited, noisy data for a limited range of scattering angles, the goals [2] and [3] can never be fully reached. As a simplification it is therefore appropriate to expand the depth dependence of $\rho^1$, $\mu^1$ and $\lambda^1$ in a suitably chosen set of basis functions $\mathbf{b}_p(z)$. The subscripts p and q are used throughout this chapter to denote these basisfunctions. The basisfunctions are used to parameterize the depth dependence of the heterogeneity, and to separate the contributions from $\rho^1$, $\mu^1$ and $\lambda^1$. From now on, we assume that the inhomogeneity can be decomposed as follows

$$\mathbf{m}(\mathbf{r})=\sum_p h_p(\mathbf{x})\,\mathbf{b}_p(z) \qquad (3.4)$$

and the aim of the inversion is to reconstruct the fields $h_p(\mathbf{x})$. The vector $\mathbf{x}$ shall be used to denote the horizontal components of $\mathbf{r}$ ($\mathbf{x}\equiv\mathbf{r}-(\mathbf{r}.\hat{\mathbf{z}})\hat{\mathbf{z}}$) this convention will be followed throughout this chapter.

In order to obtain a workable formalism, more notation needs to be introduced. A superscript "rs" shall be used to denote the source receiver pair which is considered, thus $u^{rs}(t)$ is the time signal of the recorded scattered surface wave for source "s" and receiver "r". Furthermore, let the synthetic seismogram for source receiver pair "rs", basis function $\mathbf{b}_p(z)$ and a scatterer at location $\mathbf{x}$ be denoted by $s_p^{rs}(\mathbf{x},t)$. Since the theory is linear, this synthetic seismogram is precisely the contribution of source receiver pair "rs" to the gradient ($G$) of the data at location $\mathbf{x}$ and basisfunction p.

Now let us assume that the data are uncorrelated, but that the autocorrelation of different seismograms may be different

$$C_u^{rs,r's'}(t,t') = \delta_{r,r'}\delta_{s,s'}\delta(t-t')\sigma_{rs}^2 \tag{3.5}$$

Inserting this in (3.2-3), and working out the implied operator products yields

$$h_p(\mathbf{x}) = \sum_{p_1,p_2} \int d^2x_1 \int d^2x_2\, M_{pp_1}^{-1}(\mathbf{x},\mathbf{x}_1)\, C_{m,p_1p_2}(\mathbf{x}_1,\mathbf{x}_2)\, H_{p_2}(\mathbf{x}_2) \tag{3.6}$$

where

$$H_p(\mathbf{x}) = \sum_{rs} \frac{1}{\sigma_{rs}^2} \int s_p^{rs}(\mathbf{x},t)\, u^{rs}(t)\, dt \tag{3.7}$$

and

$$M_{pq}(\mathbf{x},\mathbf{x}') = \sum_{p_1} \int d^2x_1\, C_{m,pp_1}(\mathbf{x},\mathbf{x}_1) \sum_{rs} \frac{1}{\sigma_{rs}^2} \int s_{p_1}^{rs}(\mathbf{x}_1,t)\, s_q^{rs}(\mathbf{x}',t)\, dt + \delta_{pq}\delta(\mathbf{x}-\mathbf{x}'). \tag{3.8}$$

It can be seen from (3.6) that the inversion consist of three steps. The data ($u^{rs}(t)$) enter the inversion through the "holography term" $H_p(\mathbf{x})$. After this, an integration with the model covariance ($C_m$) is performed. Finally, a contraction with the inverse operator $M^{-1}$ completes the inversion. Now let us focus on the holography term (3.7).

This term can be interpreted most easily by converting (3.7) to a frequency integral using Parseval's theorem (Butkov, 1968). Inserting (2.8) for the synthetic seismogram $s_p^{rs}(\mathbf{x},\omega)$ we get

$$H_p(\mathbf{x}) = \frac{1}{2\pi} \sum_{rs} \int d\omega \sum_{\sigma,\nu} [\mathbf{u}^{rs}.\mathbf{p}^{\sigma}(z_r)] \frac{\exp i(k_\sigma X_2 + \frac{\pi}{4})}{(\frac{\pi}{2}k_\sigma X_2)^{1/2}} V_p^{\sigma\nu}(\mathbf{x}) \frac{\exp i(k_\nu X_1 + \frac{\pi}{4})}{(\frac{\pi}{2}k_\nu X_1)^{1/2}} [\mathbf{p}^{\nu}(z_s)\cdot\mathbf{F}] \tag{3.9}$$

It is understood that all quantities at the right hand side are evaluated in the frequency domain, and that the geometric variables are to be considered for each source receiver pair separately. The interaction terms $V_p^{\sigma\nu}(\mathbf{x})$ are for scattering (and conversion) by basis function $\mathbf{b}_p(z)$ at location $\mathbf{x}$. Equation (3.9) can be interpreted by considering the terms on the left and on the right of the interaction matrix. The term $\exp i(k_\nu X_1 + \frac{\pi}{4})/(\frac{\pi}{2}k_\nu X_1)^{1/2}\ [\mathbf{p}^{\nu}(z_s).\mathbf{F}]$ describes the waves excited by the point force $\mathbf{F}$, which travel to the scatterer. In optics this term would be called "the illumination", since this term describes how much energy emanating from the source reaches the scatterer. The term $[\mathbf{u}^{rs}.\mathbf{p}^{\sigma}(z_r)]\exp i(k_\sigma X_2 + \frac{\pi}{4})/(\frac{\pi}{2}k_\sigma X_2)^{1/2}$ can be interpreted as the backpropagation of the data $\mathbf{u}^{rs}$, into the medium. This can most easily be understood by noting the symmetry in (3.9) in the excitation $\mathbf{F}$ and the data $\mathbf{u}^{rs}$. The holographic term (3.9) depends on the correlation between the illumination and the backpropagated signal. A summation over all source receiver pairs completes this term. This procedure is similar to holographic techniques in optics, where an image is reconstructed using the interference between the



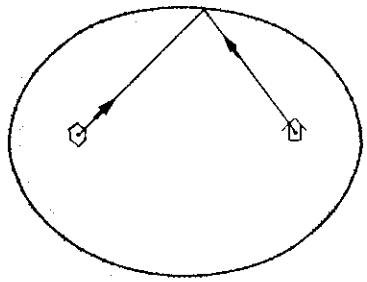

*Figure 3.* Ellipsoidal area over which the contribution of one source-receiver pair to the holographic term (3.7) is spread out in the absence of mode conversions.

illumination, and the light which has (back)propagated from the hologram to the area of reconstruction.

This holographic reconstruction procedure amounts to smearing out the recorded scattered energy over ellipses, or egg shaped curves in the medium. For instance, if mode conversions are absent, the recorded scattered wave for one source receiver pair is smeared out over an ellipse with the source and the receiver as focal points (figure 3). Using many different source receiver pairs, these ellipses are superposed to reconstruct the heterogeneity. Virtually all migration schemes used in exploration seismics use the same principle (either explicitly or implicitly). Insufficient data, or an inadequate reference model for the propagation leads to an imperfect reconstruction, producing the characteristic "smiles" in migrated seismic sections (Berkhout, 1984, chapter 5).

After applying the holographic operator in (3.6), an integration with the model covariance $C_m$ is to be applied. This covariance operator makes it possible to impose a-priori knowledge on the spatial scale of variation in the medium. The integration over $\mathbf{x}_2$ with this operator implies a smoothing of the holographic image: One should be careful not to apply too much smoothing. The reason for this is that the scattering effects are most sensitive to the horizontal gradients of the inhomogeneities. Smoothing scatterers over one wavelength of the surface waves eliminates virtually all scattering effects. Therefore it is crucial to allow sufficiently horizontal abrupt variations of the inhomogeneities.

The last step in the inversion (3.6) entails the inversion of the operator $M$ (3.8). After discretizing the model in cells, this inversion amounts to inverting a huge matrix. The matrix is in general very large, since the cell size should be much smaller than a wavelength. In order to do an inversion on a continental scale using surface waves with periods less than 100 seconds, several thousands of cells are required. A direct inversion of such a matrix is not feasible, but iterative techniques such as steepest descent, or conjugate gradients can be used for this, see chapter 1.2. Alternatively, one can complete the reconstruction (3.6) by making strongly restricting assumptions on the matrix $M$, which allows for a more convenient, but less accurate inversion of this matrix.

## 4. A simplified reconstruction procedure

In this section a simplified version of the reconstruction (3.6) is proposed. It is assumed that the heterogeneity can be described by one basisfunction $\mathbf{b}_p(z)$ and the subscript "p" is therefore dropped. Furthermore, it is assumed that the heterogeneity has a zero correlation length

$$C_m(\mathbf{x},\mathbf{x}') = \sigma_m^2\, \delta(\mathbf{x}-\mathbf{x}') \tag{4.1}$$

and that all data have the same covariance $\sigma_u^2$. Lastly, and this is the most restricting assumption, we ignore the off-diagonal elements of the operator $M(\mathbf{x},\mathbf{x}')$. In this approximation

$$h(\mathbf{x}) = M^{-1}(\mathbf{x},\mathbf{x})\, H(\mathbf{x}) \tag{4.2}$$

with

$$M(\mathbf{x},\mathbf{x}) = 1 + \frac{\sigma_m^2}{\sigma_u^2} \sum_{rs} \int s^{rs}(\mathbf{x},t)^2\, dt. \tag{4.3}$$

Assuming the operator $M$ to be diagonal means that one assumes that for each point $\mathbf{x}$, all the scattered waves for all source receiver pairs are generated by a single scatterer at location $\mathbf{x}$. This assumption clearly breaks down when different scatterers collectively generate scattered waves for all source receiver pairs. In that case (4.2-3) cannot be expected to give results which are quantitatively correct. However, it is shown in section 5 that this simplifying assumption is able to produce qualitatively meaningful results. In fact, many migration schemes used in exploration geophysics implicitly use this assumption. (As an alternative, the system (3.2-3) could be solved iteratively, as shown in Tarantola (1984ab). In that case the substitution (4.3) specifies a preconditioning parameter for the iterative inversion (Tarantola, 1984c), and the final model is insensitive to the choice of this parameter. An explicit inversion of the operator M can then be avoided.)

Combining (3.7) and (4.2-3) the image reconstruction is in this approximation

$$h(\mathbf{x}) = \frac{\sum_{rs} \int s^{rs}(\mathbf{x},t)\, u^{rs}(t)\, dt}{\frac{\sigma_u^2}{\sigma_m^2} + \sum_{rs} \int s^{rs}(\mathbf{x},t)^2\, dt} \tag{4.4}$$

The numerator is simply the holographic term. The denominator contains two terms. The autocorrelation of the synthetic seismograms in the denominator serves to normalize the reconstructed heterogeneity. The $\sigma_u^2/\sigma_m^2$ term serves to suppress the contaminating influence of noise.

It is shown in Snieder (1986ab) that the radiation pattern for surface wave scattering usually has one or more nodes. For one source receiver pair, near a node of the radiation pattern, the autocorrelation of the synthetic seismograms in the denominator approaches zero faster than crosscorrelation in the numerator. This might lead to a numerical instability. The regularization term $\sigma_u^2/\sigma_m^2$ damps this instability.



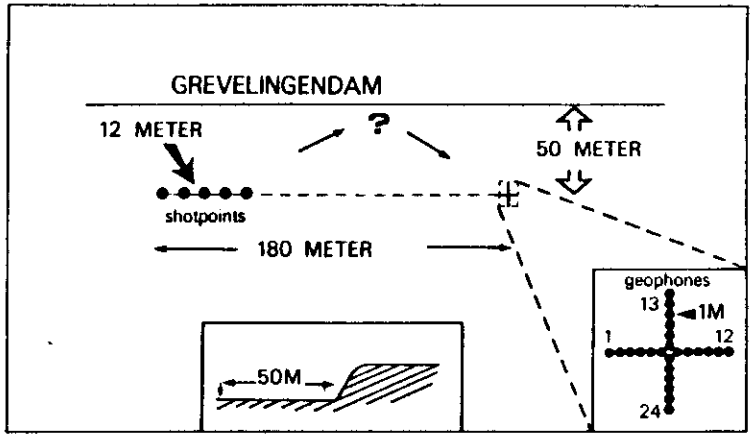


*Figure 4.* Layout of the field experiment.

## 5. A field experiment for image reconstruction with scattered surface waves

A field experiment was carried out in order the test the feasibility of surface wave holography. Surface wave measurements were done on a tidal flat in the Netherlands. A cross shaped array of 24 (10 Hz.) geophones was placed 50 meters from a concrete dam (the "Grevelingendam"). A weight drop source (of 30 kg.) was used to generate surface waves at several locations 50 meters from the dam, see figure 4. A description of the field equipment is given by Doornenbal and Helbig (1983). The reference model $(\rho_0(z), \mu_0(z), \lambda_0(z))$ used in the inversion was determined using standard surface wave dispersion analysis, using the fundamental Rayleigh modes and five higher modes (Gabriels et al., 1987).

An example of the geophone records for one shotpoint is shown in figure 5. Note the relatively strong higher mode signal before the arrival of the fundamental mode. It can be seen that the direct fundamental mode arrives simultaneously at the geophones on the transverse leg of the array (geophone 13-24), confirming that this wave propagates parallel to the dam. After this, the scattered fundamental mode arrives. On both the parallel (geophone 1-12), and the transverse (geophone 13-24) leg of the array this wave has a slanted lineup, indicating that this part of the signal comes from the direction of the dam. In this inversion the signal was muted until just after the arrival of the direct fundamental mode, so that only the scattered fundamental Rayleigh mode was used in the inversion.

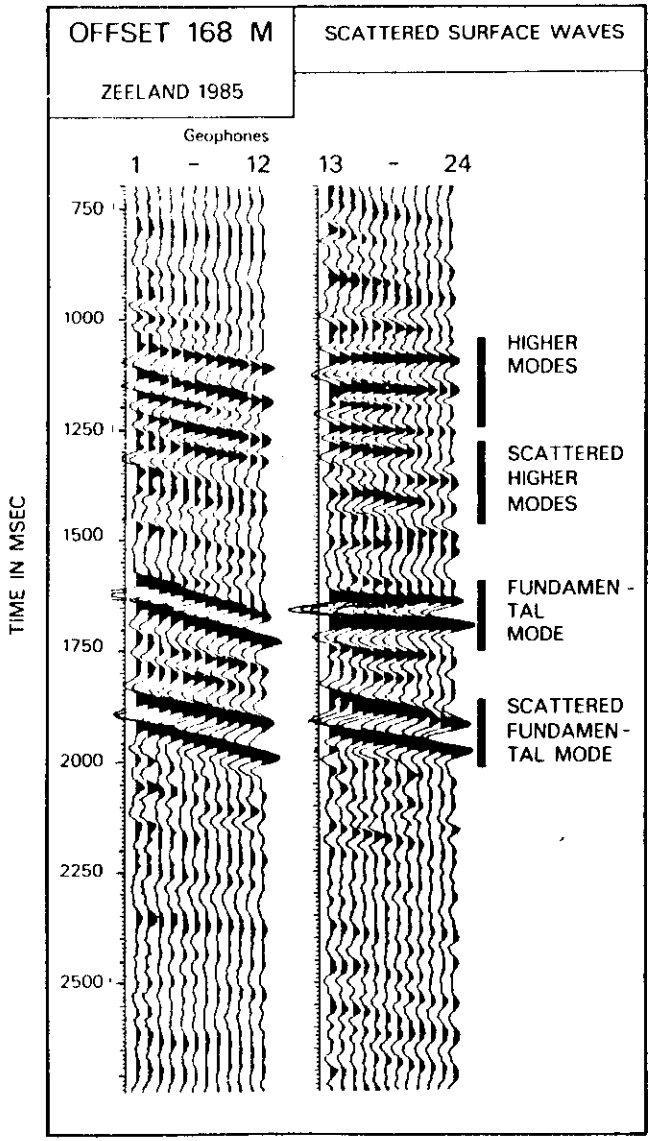


Figure 5. Field record for a shotpoint 168 meters from the geophone array.



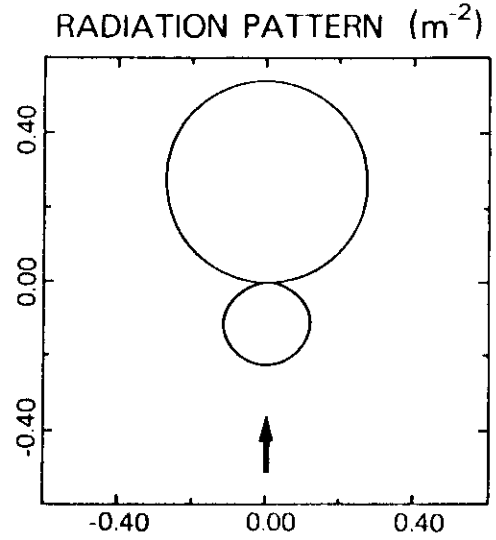


*Figure 6.* Radiation pattern for the basis function employed for the scattering of the fundamental Rayleigh mode to itself. The direction of the incoming wave is indicated by an arrow. The numbers indicate the scattering amplitude / $m^2$.

(The Love wave contribution to the data and the synthetic seismograms is zero, because a vertical force excites only Rayleigh waves, and vertical component geophones don't register Love waves.)

The sediments composing the tidal flat have a shear wave velocity of 100-300 m/sec (depending on depth), and a density of approximately 1500 $kg/m^3$. In the dam, shear wave velocities of several kilometers per second are possible, and the density can be as large as 2500 $kg/m^3$. It will be clear that the dam cannot be considered a "small perturbation", so that we cannot expect to obtain quantitatively correct information. However, the geometry of the scatterer isn't favourable to multiple scattering, which explains why this linear reconstruction technique can be employed.

As a basis function, a constant relative shear wave velocity perturbation of 500%, and a constant relative density perturbation of 25% was assumed down to a depth of 12 meters. The radiation pattern for fundamental mode Rayleigh wave scattering is shown in figure 6. Note that the radiation pattern has a node for a scattering angle of approximately 90 degrees.

The image reconstruction was performed with a straightforward numerical implementation of (4.4). The synthetic seismograms $s^{rs}(\mathbf{x},t)$ were computed in the frequency domain using (2.8), and then Fourier transformed. Imaging experiments were

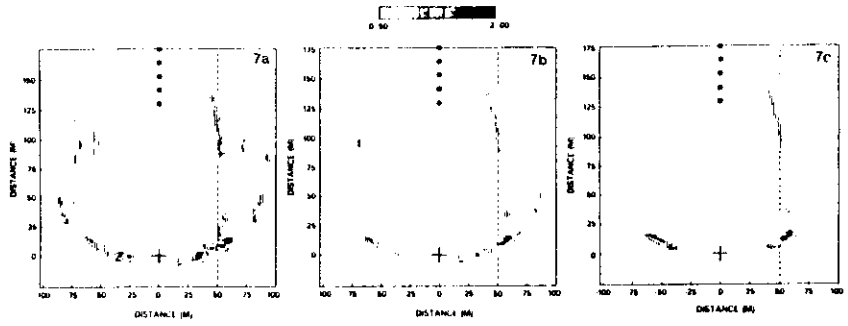


*Figure 7a*. Envelope of the reconstructed image $h(x)$ in the undamped case ($\sigma_u=0$), using only 4 geophones of the array. The true location of the edge of the dam is shown by the vertical dashed line. The shotpoints and the geophone array are marked with dots and a cross.
*Figure 7b*. As figure 7a, using only 8 geophones of the array.
*Figure 7c*. As figure 7c, using all 24 geophones of the array.

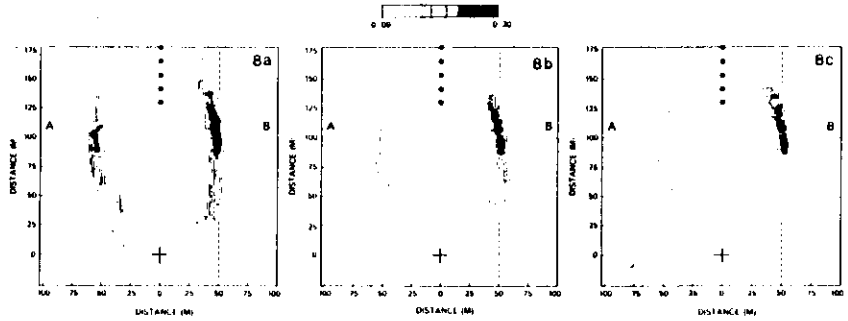


*Figure 8a*. Envelope of the reconstructed image $h(x)$ in the damped case ($\sigma_u\neq0$), using only 4 geophones of the array. The true location of the edge of the dam is shown by the vertical dashed line. The shotpoints and the geophone array are marked with dots and a cross.
*Figure 8b*. As figure 8a, using only 8 geophones of the array.
*Figure 8c*. As figure 8c, using all 24 geophones of the array.

performed for geophone spacings of 6 meters (using 4 geophones), 3 meters (using 8 geophones) and 1 meter (using all geophones). (The dominant wavelength of the fundamental Rayleigh mode is 6 m.) In all cases five shotpoints were used in the inversion. The reconstructed inhomogeneity is a highly oscillatory function of the space variables, since the reconstructed inhomogeneity $h(x)$ consists of the temporal correlation of two dispersed wavetrains. In the results presented here, the envelope of the function $h(x)$ is



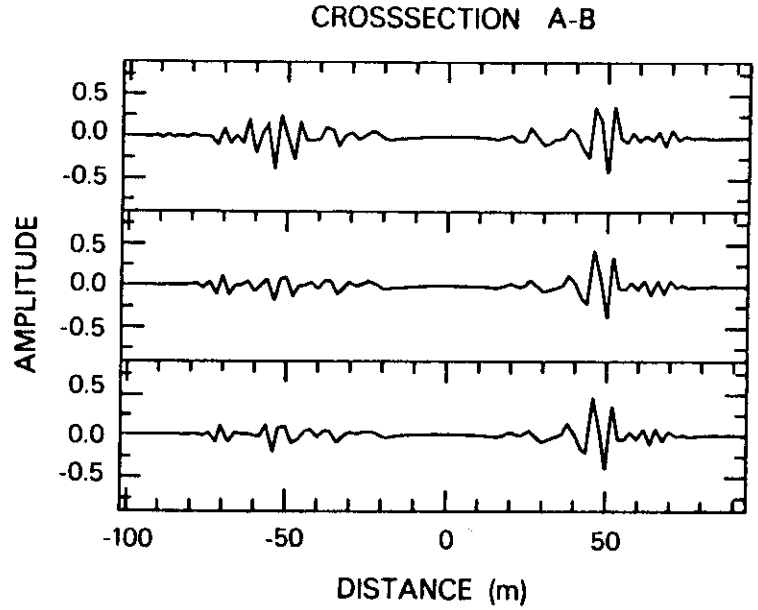


*Figure 9*. Cross sections of the reconstructed image $h(x)$ along the line AB for the solution in figure 8a (top panel), figure 8b (middle panel) and figure 8c (bottom panel).

therefore shown. In the figures 7a,b,c the reconstructed image is shown in the undamped case ($\sigma_u=0$) for different geophone spacings. The dam is not reconstructed very well, and the reconstructed heterogeneity is dominated by a sickle shaped body near the geophone array. This is caused by the fact that for the basis function employed here, the radiation pattern has a node near 90 degrees, see figure 6. Therefore, all the points near the circle with the source and the receiver as antipodal points produce a scattered wave $s^{rs}(x,t)$ with very small amplitude. Since the denominator in (4.4) goes faster to zero with $s^{rs}(x,t)$ than the numerator, this leads to an unrealistic inhomogeneity where these circles for different source receiver pairs overlap. This happens close to the geophone array. Taking more geophones into account gives some improvement, but the result isn't very good.

If the damping is nonzero ($\sigma_u\neq0$), the results are considerably better, as can be seen in the figures 8abc. The sickle-shaped "ghost heterogeneity" has disappeared, and in all cases a clear image of the dam is visible at the correct location. In all cases a mirror image of the dam (at the left side of the shotpoint-geophone line) is visible, but if more source receiver pairs are taken into account this mirror image weakens. The reason for this is that only the geophones on the transverse leg of the array contribute to a determination between "left and right" for the incoming waves. Taking more geophones into account leads to a better determination of the direction of the incoming wave.

Note that with a geophone spacing comparable to the dominant wavelength (as in figure 8a), the inhomogeneity can still be reconstructed. This is fortunate, because in global seismology the station density is usually so small that the stations are more than a wavelength apart. Apparently, spatial aliasing effects don't affect the reconstruction strongly.

Cross sections of the field $h(\mathbf{x})$ along the line AB in figures 8abc are shown in figure 9 for the three geophone spacings employed. Note the oscillatory character of the reconstructed image, which is a by-product of the correlation technique used here. The image of the dam can clearly be seen at 50 meters. The mirror image of the dam is also visible, but it can be seen that using more geophones leads to a weakening of this mirror image. Unfortunately, it is not possible to determine the sign of the heterogeneity from figure 9. In reality, the inhomogeneity is certainly positive because both the shear wave velocity and the density are much higher in the dam than in the tidal flat. Due to the oscillatory character of the reconstructed image this cannot be determined from figure 9. This experiment has shown the feasibility of locating lateral heterogeneities in the Earth using scattered surface waves. Application of this technique to seismological data recorded with the NARS array (Dost et al., 1984) is currently in progress.

*Acknowledgements.* I am much indebted to Guust Nolet, both for proposing the field experiment as well as for his continuous interest and advice. Wout Brouwer helped developing the software for the data analysis. K. Helbig and Johan Tempels from the Department of Exploration Geophysics of the University of Utrecht kindly lent us their field equipment and provided technical assistance.